Journal Pre-proof

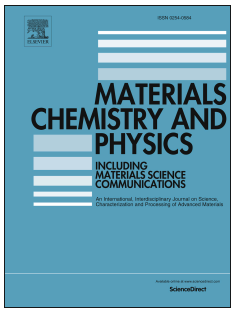

Targeted dielectric coating of silver nanoparticles with silica to manipulate optical properties for metasurface applications

Z. Lalegani, S.A. Seyyed Ebrahimi, B. Hamawandi, L. La Spada, H. Batili, M.S. Toprak

PII: S0254-0584(22)00556-9

DOI: https://doi.org/10.1016/j.matchemphys.2022.126250

Reference: MAC 126250

To appear in: *Materials Chemistry and Physics*

Received Date: 5 January 2021

Revised Date: 5 April 2022

Accepted Date: 9 May 2022

Please cite this article as: Z. Lalegani, S.A.S. Ebrahimi, B. Hamawandi, L. La Spada, H. Batili, M.S. Toprak, Targeted dielectric coating of silver nanoparticles with silica to manipulate optical properties for metasurface applications, *Materials Chemistry and Physics* (2022), doi: https://doi.org/10.1016/j.matchemphys.2022.126250.

Targeted Dielectric Coating of Silver Nanoparticles with Silica to Manipulate Optical Properties for Metasurface Applications

Z. Lalegani[1], S.A. Seyyed Ebrahimi[1*], B. Hamawandi[2], L. La Spada[3], H. Batili[2], M. S. Toprak[2**]

[1]Advanced Magnetic Materials Research Center, School of Metallurgy and Materials, College of Engineering, University of Tehran, Tehran, 11155 4563, Iran

[2]Department of Applied Physics, KTH Royal Institute of Technology, SE- 106 91 Stockholm, Sweden

[3]School of Engineering and the Built Environment, Edinburgh Napier University, Edinburgh, United Kingdom

[*]*Corresponding author e-mail: saseyyed@ut.ac.ir*

[**]*Corresponding author e-mail: toprak@kth.se*

Abstract

An epsilon-negative metamaterial (ENM) containing core@shell nanoparticles (NPs) was designed, where silver (Ag) NPs served as core and silica (SiO_2) was used as spacer shell. AgNPs were synthesized in large scale, using microwave-assisted polyol method, in three average particle sizes, as 30, 54, and 61 nm, with a narrow particle size distribution. Optical absorption of Ag NPs was investigated using UV-Vis spectroscopy. Their optical behavior was also theoretically predicted for different thicknesses of the SiO_2 shell immersed in media of different refractive indices using the Clausius - Mossotti equation. Based on the results, optimal outputs were obtained with a SiO_2 shell of 10 nm in thickness encompassing 54nm Ag NPs based on the analytical model and numerical simulations here developed for core-shell structures. Then 10 nm SiO_2 shell was grown on 54 nm Ag NPs by sol-gel synthesis. The NPs were then characterized by UV-Vis, TEM, SEM, EDX, DLS, and zeta potential analyses. The synthesized core-shell NPs can be used to establish epsilon-negative properties in polymer layers within visible range of wavelengths.

Keyword: Epsilon-negative; core-shell nanoparticles; Silver; metamaterials; Ag@SiO_2

1. Introduction

The resonant absorption and light dispersion resulted from the coherent oscillations of free electrons within the conductivity band provide the nanoparticles (NPs) of noble metals with such unique properties that are virtually absent in their bulk state, contributing to increased intensity of localized electric field near the surface of the NPs [1]. Especially for the gold (Au) and silver (Ag), the plasmonic effect of the NPs has promoted the research on the optical applications of such NPs, including those in solar cells, photocatalysts, sensors, and metamaterials [2-6], making the plasmonic effect an interesting field of the modern research.

Among other noble metals, Ag is not only advantageous in terms of price and physicochemical properties, but it also provides a molar damping coefficient that is 100 times larger than that of Au, making its NPs the material of choice for optical applications [7]. Ag NPs can be considered as the building block of new matters with special characteristics. The synthesis of these NPs at large scale with uniform particle properties was a major challenge in the nanotechnology until recently. We addressed this difficulty by formulating a simple yet robust procedure that was used to obtain large amounts of uniform Ag NPs per batch using MW-assisted polyol synthesis route [8]. Despite the widespread application of the Ag NPs in the optical materials, their tendency toward aggregation in long-term and high sensitivity to oxidation have made them incompatible with particular applications. The solution to this has been to coat their surface with a kind of protective and robust layer.

Development of an oxide shell around the metal cores can not only serves to protect them, but also provides their hybrid structure with new advantageous features [9]. One of the best oxides for such a purpose is silica (SiO_2), which is a stable and chemically inert species that can protect the Ag cores against the ions in other media [10] and contributes to better control of the spacing between the Ag cores. The coating of Ag NPs with a SiO_2 shell generates a controlled dielectric medium around the Ag NPs, making them suited for optical applications. An interesting application of the Ag@SiO_2 NPs in the field of biotechnology is the metal-enhanced fluorescence (MEF) phenomenon. Resulted from the plasmon coupling between the metallic nanostructures and fluorophores [11], the MEF can add to the luminance lifetime of particular complexes while decreasing and increasing the nonradiative and radiative transmission rates, respectively [12-14]. The Ag@SiO_2 NPs can also be used in the newly introduced MEF-based biosensing platforms [15, 16].

For the Ag NPs, the interparticle spacing plays a crucial role in the intensification of the electric field. Indeed, in a structure with closely spaced NPs, the electromagnetic fields can be effectively localized to establish hotspots in the spacing between the NPs. This is highly advantageous for the design of plasmonic systems with highly localized electric fields for sensing application [17, 18]. Niciński *et al.* [19] proposed a surface-enhanced Raman scattering (SERS)-active platform coupled with a microfluidic device containing Ag@SiO_2 NPs. In principle, the system worked based on the intensification of electromagnetic field, where the Ag@SiO_2 NPs were used to enhance the detection sensitivity of the tumor cells.

Metamaterials represent another area of interest in the fields of the material physics, optics and engineering: materials of special electromagnetic properties that cannot be achieved in natural media. The metal/dielectric core-shell NPs have been a major candidate for being

used as meta-atom for designing and manufacturing the metamaterials [20] and advanced and new NPs properties.

In order to use the $Ag@SiO_2$ NPs in the mentioned optical applications, it is crucial to design the structures hosting the NPs with optimal geometry. In the present work, optimum geometry of the Ag NPs was obtained for designing an epsilon-negative metamaterial structure, containing the $Ag@SiO_2$ NPs. A new analytical model has been developed and SiO_2 coating has been performed using Stöber process to obtain $Ag@SiO_2$ core-shell NPs of appropriate size.

2. Analytical model and design of core-shell NPs

In this paragraph we develop a new analytical formulation for the effective polarizability of a multi-layer structure and applied such formula for modelling and design the effective constitutive parameters of core-shell spherical nanoparticles. Figure 1a shows the structure under study: it consists of a generic inclusion with electric permittivity ε_1, embedded in a dielectric bounded environment of permittivity ε_2. To study its electromagnetic properties, the following assumptions must be made:

• The inclusion is much smaller than the operative wavelength and the electromagnetic field is approximately constant over the particle volume. Therefore, quasi-static approximation can be used to study the resonant behaviour of the individual structure [21].

• The considered particles and the surrounding material are homogeneous and isotropic. The surrounding material is a non-absorbing medium [22].

To make a relation between the macroscopic electromagnetic behavior of a particle embedded in a host medium and its effective polarizability we can use the following equation [23]:

$$\alpha = \frac{V\varepsilon_2(\varepsilon_1 - \varepsilon_2)}{\varepsilon_2 + L(\varepsilon_1 - \varepsilon_2)} \qquad (1)$$

where L and V are the depolarization factor and volume of the particle, respectively.

In our case, it was considered a particle embedded in a bounded homogeneous medium with the dielectric permittivity ε_2 (Figure 1a). If the average polarizability of the particle 1 is α_{av1}, consequently, it can be defined its average dielectric polarizability as:

$$\alpha_{av1} = \frac{V_1\varepsilon_2(\varepsilon_{av1} - \varepsilon_2)}{\varepsilon_2 + L_1(\varepsilon_{av1} - \varepsilon_2)} \qquad (2)$$

Now let's assume that the aforementioned particle (α_{av1}) is surrounded by a dielectric layer of permittivity ε_2 (Figure 1a). We have to find the polarizability of the covered particle. To address this issue, the initial particle is placed in a homogeneous dielectric medium with permittivity ε_2 and then surround the initial particle by an imagine particle, as depicted in Figure 1b. Now this imagine particle is replaced by a homogeneous particle with the average polarizability α_{av2} (Figure 1c) and:

$$\alpha_{av2} = \frac{V_2\varepsilon_2(\varepsilon_{av2} - \varepsilon_2)}{\varepsilon_2 + L_2(\varepsilon_{av2} - \varepsilon_2)} \qquad (3)$$

Which provide an equivalent dipole moment and polarizability for the particle in Figure 1b. Consequently, we have:

$$\alpha_{av1} = \alpha_{av2} \qquad (4)$$

$$\frac{V_1\varepsilon_2(\varepsilon_{av1} - \varepsilon_2)}{\varepsilon_2 + L_1(\varepsilon_{av1} - \varepsilon_2)} = \frac{V_2\varepsilon_2(\varepsilon_{av2} - \varepsilon_2)}{\varepsilon_2 + L_2(\varepsilon_{av2} - \varepsilon_2)} \qquad (5)$$

By solving respect to α_{av2}, a new relationship for the effective polarizability (and therefore the effective permittivity) is obtained, to design/retrieve the values of the effective constitutive parameters of the layered structure under study (Figure 1d).

$$\alpha_{eff} = \frac{\varepsilon_2\left(V_1(L_2 - 1)(\varepsilon_2 - \varepsilon_1) + V_2\big(L_1\varepsilon_1 - \varepsilon_2(L_1 - 1)\big)\right)}{L_2V_1(\varepsilon_2 - \varepsilon_1) + V_2\big(L_1\varepsilon_1 - \varepsilon_2(L_1 - 1)\big)} \qquad (6)$$

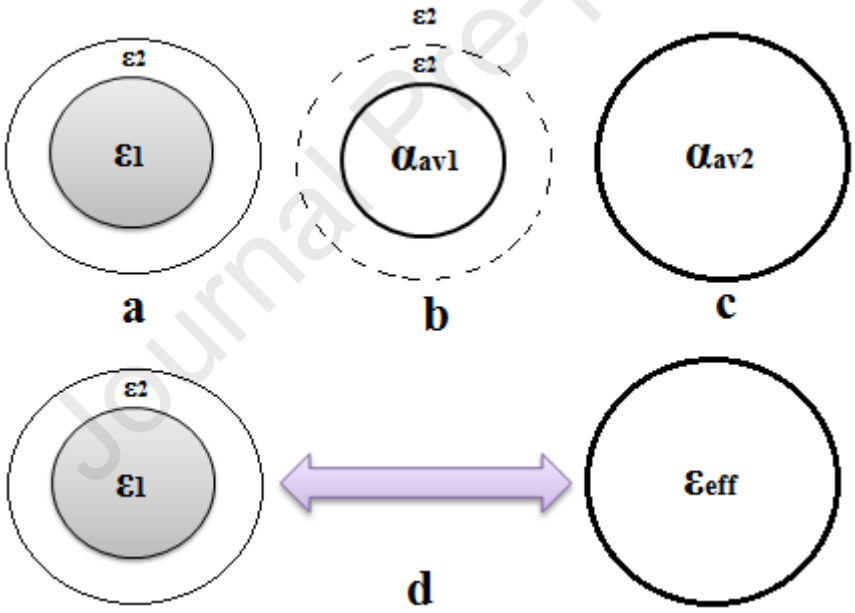

Figure 1: a) Original layered particle with permittivity ε_1 and ε_2 for the core and the shell, respectively; b) fictional particle with polarizability α_{av1} immersed in a surrounding medium of permittivity ε_2; c) single particle with average polarizability α_{av2}; and d) single particle with polarizability α_{eff}, equivalent to original layered particle (ε_1 and ε_2).

3. Experimental

3.1. Materials and instrumentation

Silver nitrate ($AgNO_3$, crystal extra pure, Merck, Sweden), polyvinyl pyrrolidone –PVP (K30, PanReacAppliChem), and ethylene glycol –EG ($C_2H_6O_2$, Sigma Aldrich, Sweden)

were used as Ag precursor, capping agent, and reducing solvent, respectively. As for the SiO_2 coating, tetraethyl orthosilicate (TEOS, $Si(OC_2H_5)_4$, Sigma Aldrich, Sweden), ammonium hydroxide (NH_4OH, Sigma Aldrich, Sweden), and ethanol (Sigma Aldrich, Sweden) were used as SiO_2 precursor, catalyst, and solvent, respectively.

Morphology of Ag@SiO_2 NPs was characterized using transmission electron microscopy (TEM, JEM-2100F, 200 kV, JEOL Ltd. Tokyo Japan) and scanning electron microscopy (SEM- FEI Nova200, Hillsboro, OR, USA). The energy dispersive spectroscopy (EDS) was used to analysis of chemical composition of the NPs. Average size of NPs was measured using ImageJ software and dynamic light scattering (DLS- Malvern Zetasizer Nano ZS90). UV-Vis spectrophotometry (ImplenNanoPhotometer, NP80) was used to determine the SPR spectra of AgNPs and Ag@SiO_2 NPs. In order to obtain the desired effective dielectric constant according to the Clausius–Mossotti relation, the central composite design (Response surface – CCD; Design expert software (DOE; version 11.0.3.0, Stat – Ease, USA)) was used.

3.2. Synthesis of Ag NPs

The Ag NPs were synthesized via the microwave-assisted (MW-assisted) polyol method, as thoroughly described in our recent work [8]. In brief, appropriate amounts of $AgNO_3$ and PVP were dissolved in 40 mL of EG and transferred to a MW reaction chamber. Utilizing the MW-assisted heating, the solutions were heated to 145°C in 1 min, with their temperature kept there for another 2 min before cooling down to room temperature. As a result of this synthesis procedure, Ag NPs of 30, 54, and 61 nm in size were produced from different amounts of precursor as listed in Table S1.

3.3. Synthesis of SiO_2 coated Ag (core-shell Ag@SiO_2) NPs

The Stöber process [24, 25] was utilized to synthesize the Ag@SiO_2 core-shell NPs in this research, which is based on sol-gel SiO_2 formation in alcoholic solution with the catalysis of a base. In a typical process, 1 mL of a solution composed of ethanol and 0.0012 g of Ag NPs with an average particle size of 54 nm was added to 40 mL of ethanol in a 100 mL round-bottom flask under stirring, and the mixture was further stirred for 10 min. Subsequently, keeping the solution under stirring, 1.5 mL of ammonium hydroxide was added to adjust the solution pH to 10. Afterwards, 2 µL of TEOS was introduced into the solution and the flask was sealed for 18 h under stirring. The solution was then transferred into a 40 mL vial and subjected to centrifugation at 12,000 rpm for 15 min, upon which stage the core-shell NPs were precipitated and collected for further analysis without needing additional washing steps. Thus, the core-shell Ag@SiO_2 NPs, where 54 nm Ag NP coated with 10 nm SiO_2 shell were obtained.

4. Results and discussion

4.1. Optical characteristics of the synthesized Ag NPs

Three samples of Ag NPs were synthesized with average particle size of 30, 54, and 61 nm. SEM images of the NPs are displayed in Figure S1, indicating the spherical geometry and

narrow particle size distribution of the NPs. Figure 2 displays a typical Ag NP and confirms the high crystallinity through the fourier transform (FFT) image presented alongside.

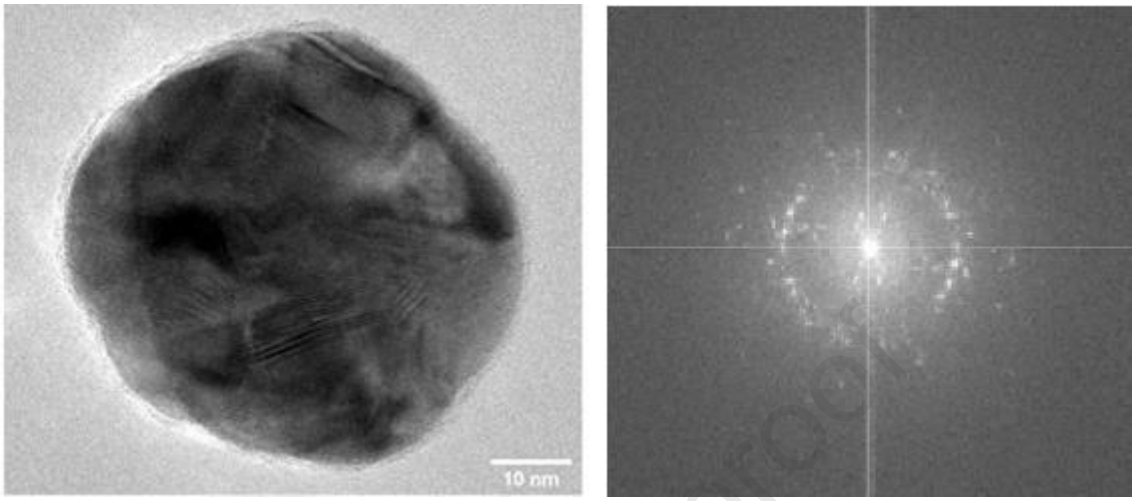

Figure 2: TEM micrograph and FFT of Ag NPs.

UV-Vis spectroscopy was conducted to evaluate the optical characteristics of the synthesized Ag NPs, with the results shown in Figure 3. The UV-Vis spectra showed a single absorption band called the Ag plasmon peak. Mie was not the first to formulate the electromagnetic dispersion, but his well-known theory (the Mie theory) can well explain the SPR of the highly symmetric Ag NPs when their size is comparable to the incident electromagnetic ray wavelength [26-28].

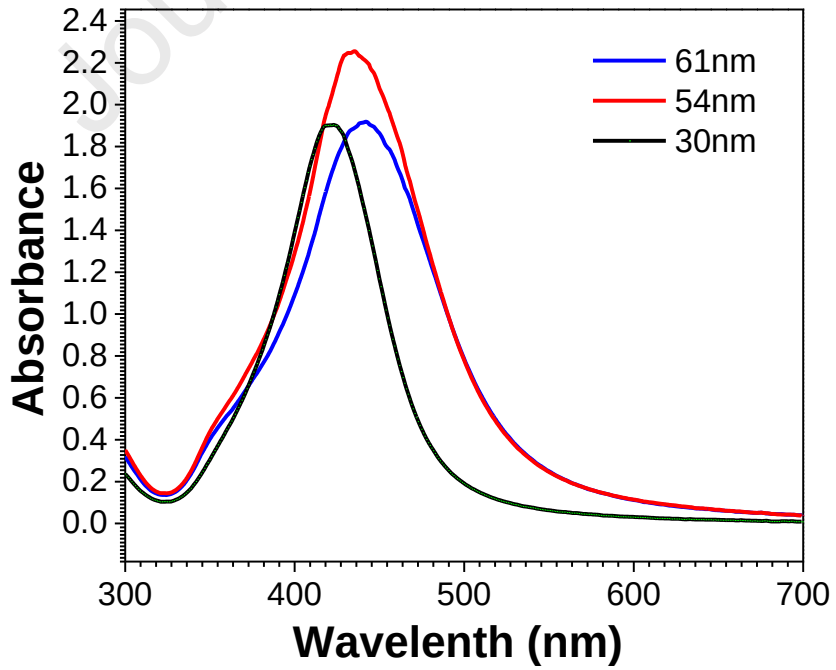

Figure 3: UV-Vis spectra of Ag NP samples with average particle size of 30, 54, and 61nm.

Resulted from collective oscillation of surface electrons, the optical absorption and dispersion of Ag NPs are known as surface plasmon. When the frequency of oscillation of these electrons coincides with that of the electromagnetic ray, the resonance condition is established. In nanostructures of Ag, this is called localized surface plasmon resonance (LSPR) [29-31]. A large metallic crystal exhibits an absorption peak at zero frequency but, according to the Mie theory, the absorption peak frequency may shift to visible or near UV region if the particle size is small compared to the incident light wavelength [32]. For the Ag NPs, the absorption peak wavelength ranges from about 400 nm to 530 nm, with the actual extent of shift being dependent on the particle size and shape, and the dielectric medium encompassing the particle [31, 33]. Considering Figure 3, the resonance absorption peak was observed at 422, 436, and 442 nm for the Ag NPs with average particle diameters of 30, 54, and 61 nm, respectively. These were resulted from the excitation of the surface plasmon oscillations and, as observed, the absorption peaks exhibited a red-shift with increasing the average size of the Ag NPs. These collective excitations and the red-shift can be interpreted by the modified Drude model, which presents the following equation for predicting the permittivity which imposes a crucial contribution to the LSRP properties for the NPs larger than 10 nm in average diameter [34]:

$$\varepsilon_{NP}(\omega, r) = \varepsilon_{bulk}(\omega) + \frac{\omega_P^2}{\omega^2 + i\Gamma_0\omega} - \frac{\omega_P^2}{\omega^2 + i\,\Gamma(r)\omega} \qquad (7)$$

Where ω_p is the electron density-dependent plasma frequency and $\Gamma(r)$ is the modified damping frequency of the NPs – a parameter that is dependent on the particle size. Therefore, it can be understood that the shift of the resonance peak depends on the density of the near surface free electrons of the Ag NPs. Since an increase in the particle size extends the electron density profile, then such an increase enhances the polarizability and hence lowers the resonance frequency. Tiggesbäumker *et al.* [35] referred to the red-shift as a spill-out effect, introducing it as an intrinsically dynamic effect. Hilger *et al.* [36], on the other hand, stipulated that the difference in the added mass because of the increased size cannot justify the red-shift, referring to the change in the electromagnetic coupling as the main cause of the shift. As the average diameter of the Ag NPs increases, the spacing between the surface charges extends, lowering their interactions and hence the restoring forces, which eventually leads to the red-shift of the plasmon absorption peak [37].

According to Figure 3, as the average particle size increased from 30 nm to 61 nm, the full width at half maximum (FWHM) increased by 31 nm, which could be a result of either the nonuniform polarization of the larger NPs in the electromagnetic field of the incident ray or the excitations induced by the quadrupolar or octopolar modes, which is usually referred to as non-inherent effect of size and holds true for particles with sizes larger than 20 nm [38].

These unique properties of the Ag NPs, which are most commonly resulted from small overlapping between the SPR and inter-band transitions in the Ag, have made them exhibit a more intensive plasmonic resonance in the range of visible wavelengths, as compared to other

noble metals [26]. Nevertheless, incorporation of Ag NPs into applicable parts is difficult because of not only their tendency towards aggregation by the Van der Waals forces in the long time, but also the sensitivity of the Ag to the surrounding chemical medium and its susceptibility to oxidation and degradation of its plasmonic properties. In order to cope with this problem and to engineer NPs plasmonic behavior, it is necessary to establish a stable coating on the surface of the Ag NPs [7, 39, 40]. In the present work, optimal usage of the synthesized Ag NPs in plasmonic parts was sought by coating the particles with SiO_2 – a very stable material against environmental changes in many chemical media. First, appropriate thickness of the SiO_2 coating was designed to obtain the desired properties for the considered application. Then, attempts were made to synthesize core-shell Ag@SiO_2 NPs with the designed dimensions.

4.2. Parameters affecting the optical response of the synthesized Ag NPs for the design of the metasurface

Optical response of the randomly arranged dipolar particles can be investigated by the Clausius - Mossotti equation, which expresses the relationship among the effective permittivity and permeability with the polarizability and volumetric fraction of the particles, *f*, as follows [20]:

$$\frac{\varepsilon_{eff} - \varepsilon_{\circ}}{\varepsilon_{eff} + 2\varepsilon_{\circ}} = f\frac{\alpha_{eff}}{4\pi r^3} \qquad (8)$$

Where α_{eff} is the effective electrical polarizability of spherical particles ($L = \frac{1}{3}, V = \frac{4}{3}\pi r^3$) in formula (6), and *r* is the radius of particles.

In the present work, the parameters affecting the ε_{eff} were investigated to design a metasurface with negative or near-zero epsilon. In order to determine the relationship between the parameters affecting the ε_{eff}, the Clausius - Mossotti equation was designed via Central Composite Designs (CCD) to obtain an approximate map of the effects of different parameters on the ε_{eff}. The required optical data were extracted from the refractive index database [41] based on Malitson [42] and McPeak *et al*. [43]. The optical data in details are listed in Table S2. Here the following parameters were selected as independent variables: wavelength, core (Ag) radius, shell (SiO_2) thickness, filling factor, and refractive index of the host medium. These parameters together with their considered levels are listed in Table 1. In this work, the filling factor, *f*, shall mean the volumetric fraction of the core-shell NPs in a rectangular polymer layer, *i.e.* the host medium. The reason behind using a thin shell of SiO_2 in this design was the fact that larger Ag NPs with a relatively thin dielectric coating can exhibit cooperative effects with the adjacent Ag NPs, which means the overlapping of the localized electromagnetic fields. This while a thicker shell (equal to the diameter of the Ag NPs) masks the effect of the host medium surrounding the Ag@SiO_2 NPs completely [44].

Table 1: Selected factors and their levels for Clausius-Mossotti equation

Factor	Name	Units	Type	Minimum	Maximum	Coded Low	Coded High	Mean
A	Wavelength	nm	Numeric	300	1000	-1 ↔ 475	+1 ↔ 825	650
B	Core radius	nm	Numeric	15	50	-1 ↔ 23.75	+1 ↔ 41.25	32.50
C	Shell thickness	nm	Numeric	0	20	-1 ↔ 5	+1 ↔ 15	10
D	Filling factor		Numeric	0.1	0.7	-1 ↔ 0.25	+1 ↔ 0.55	0.4
E	Refractive index of the host		Numeric	1	1.5	-1 ↔ 1.13	+1 ↔ 1.38	1.25

The experiments designed with various parameters are presented in Table S3. Selected as the response, the parameter $\varepsilon_{eff}$was theoretically obtained from the Clausius - Mossotti equation, as per corresponding coding in Matlab. Utilizing the Matlab, the real and imaginary parts of the ε_{eff} were calculated, with the real part reported as epsilon in Table S3. This preliminary design was conducted to simplify the use of the Clausius - Mossotti equation for investigating the interplay between different parameters and subsequently designing the desired metasurface. The 2D and 3D maps presented in Figure 4 show the effects of the independent variables on the response.

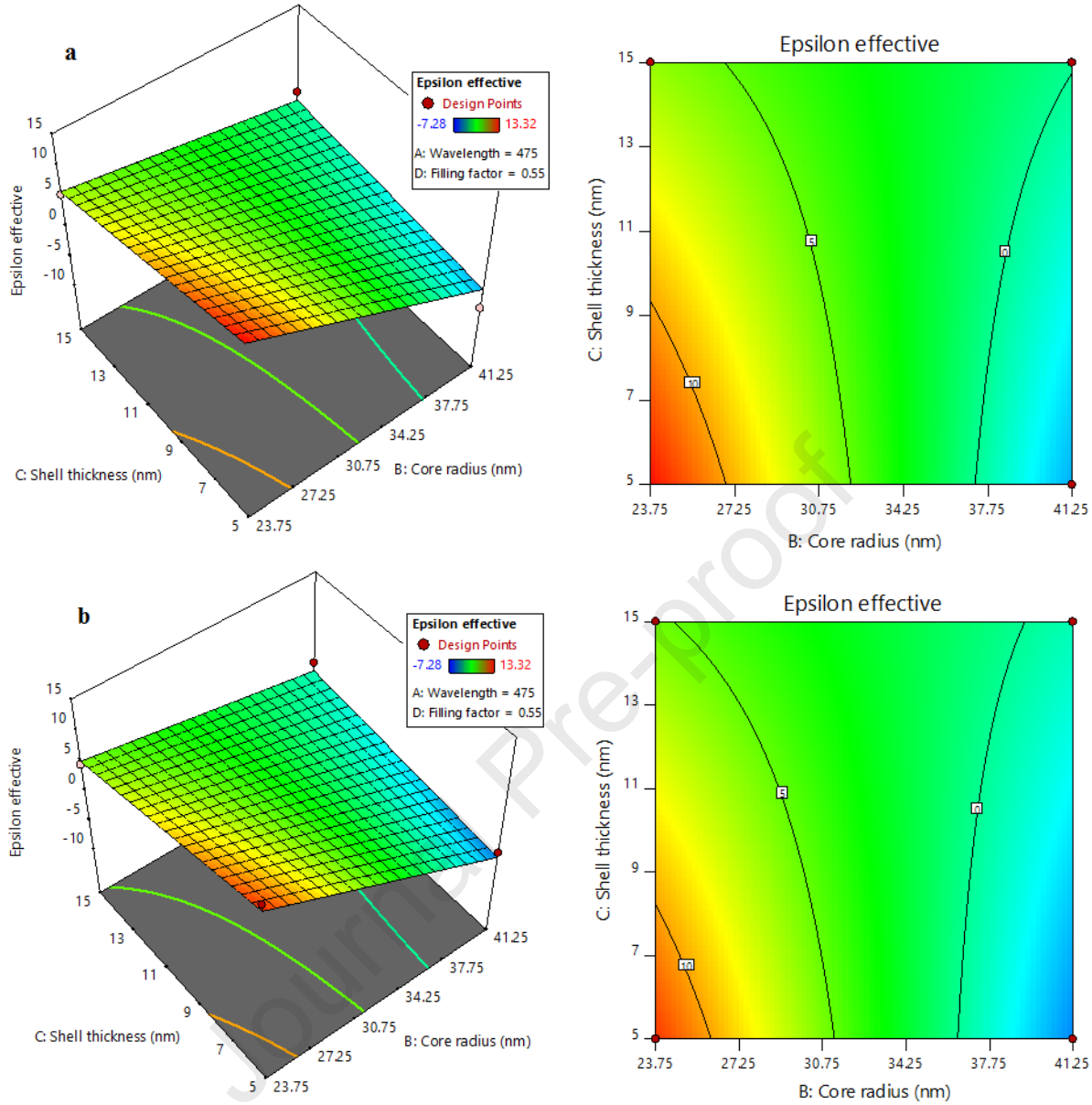

Figure 4: Contour and 3D plots showing the combined effect of core radius and shell thickness in a host medium with refractive index of 1.375 (a), the combined effect of core radius and shell thickness in a host medium with refractive index of 1.125 (b) on the ε_{eff} of Ag@SiO_2/polymer composites.

According to Figure 4a in the visible range of spectrum and with f = 0.55, the epsilon-negative metasurfaces (ENMs) could be obtained with increasing the Ag core size, with the range limited and disappeared with decreasing the f down to 0.25 (Figure S2a and S2b). Figure 4b shows that a wider range of ENM could be expected if the refractive index of the host medium is reduced. On the other hand, in a low-refractive index host medium, one could anticipate increased epsilon with lowering the f (Figure S2c). A clear conclusion is the significant effect of the refractive index of the host medium on the ε_{eff}. This is because of the establishment of a constant charge density called damped non-propagated waves due to

incompliance of the wave impedances in the shell and the host medium as a result of the polarization of the incident field and the electric field induced by the dipolar plasmon of the core [29]. Pal *et al.* [29] suggested that when the dielectric constant of the medium wherein the NPs disperse is equal or very close to that of the shell matrix, the contribution of the dispersion medium is larger and the near electric field (NEF) is intensified along their interface. Based on Figure 4a and b, an increase in the shell thickness from 5nm to 15nm eases the achievement of near-zero and negative ε. Therefore, based on the obtained results, it is likely that a thickness of 10 nm for the SiO_2 shell on the 54nm Ag NPs can lead to the desired properties for the considered metasurface. The next section describes the efforts made to develop a 10nm shell on the surface of Ag NPs and discusses the properties of the obtained core-shell NPs.

4.3. Coating the silica on the Ag NPs

The Stöber process was used to coat the Ag NPs with a 10nm shell of SiO_2. This process includes the hydrolysis and condensation of a silicon (Si) alkoxide in an alcoholic solution in the presence of a catalyst, which leads to the growth of SiO_2 on the surface of the NPs, with the growth being dependent on the competition between the rates of diffusion, hydrolysis, and condensation of the SiO_2 precursor as well as the surface chemistry of the NPs [45]. TEOS used as SiO_2 precursor, ethanol as an alcoholic solvent, and ammonium hydroxide as the catalyst. Hydrolysis of TEOS was performed via the following reaction in the presence of water:

$$Si(OC_2H_5)_4 + 4H_2O \rightarrow Si(OH)_4 + 4C_2H_5OH \qquad (9)$$

Considering the above-expressed reaction, the hydrolysis process depends on the water-to-TEOS molar ratio. Donatti *et al.* [46] proved that the TEOS reacts completely at a water-to-TEOS molar ratio≥ 4, while a poly-condensation reaction occurs at ratios lower than 4 to produce the required water for the continuation of the hydrolysis process. In this work, we did not use the water directly for the coating process as the water content of the ammonium hydroxide was large enough to have the TEOS hydrolyzed completely. When an ethoxide group (OC_2H_5) is exchanged with a hydroxyl group (OH), the electron density of the Si decreases, accelerating the rate at which other ethoxide groups are being hydrolyzed [47]. Indeed, by avoiding the direct use of water, we could lower the rate of hydrolysis and prevent the shell formation on multiple cores simultaneously. Condensation of $Si(OH)_4$ occurred concurrently with the hydrolysis, resulting in the formation of a SiO_2 shell around the Ag NPs through the following reaction:

$$Si(OH)_4 \rightarrow SiO_2 + 2H_2O \qquad (10)$$

The shell formation depends on various parameters including the pH, temperature, type of solvent, and surface chemistry of the NPs [48]. Synthetic polymers can, through the steric stabilization mechanism, play significant roles in controlling the surface chemistry and successful coating of SiO_2 on the NPs [49]. An important example of such polymers is the PVP, which can serve as a surface priming agent to replace the SiO_2 shell. The Ag NPs synthesized in the present study were provided with a PVP layer that kept the NPs in the

suspension while being transmitted into the alcoholic solvent, preventing the aggregation of the NPs and degradation of the desired properties. Ethanol was selected as the alcoholic solvent due to its relatively low hydrolysis rate which made it suitable for the formation of the SiO_2 shell on the larger Ag NPs. Niitsoo *et al.* [44] investigated the formation of $Ag@SiO_2$ NPs in different alcoholic solvents and suggested that the formation of the $Ag@SiO_2$ core-shell NPs in ethanol is controlled by the surface area of the Ag, and explained the non-formation of such core-shell complex in methanol by the high hydrolysis rate of the solvent, which led to the rapid formation of small and electrostatically stable particles of SiO_2. Therefore, the nucleation of the SiO_2 in the ethanol occurred heterogeneously, where the Ag NPs had their entire surface well coated with the SiO_2 shell. Thickness of the SiO_2 shell is highly affected by the concentration of the TEOS and the reaction time.

An important advantage of the SiO_2 shell on the Ag NPs is the attenuation of the interface issues resulted from the crystal defects that would otherwise end up with a high charge-carrier recombination rate [50]. As shown in Figure 5a, we could successfully block the surface of the Ag NPs physically. Figure 5a demonstrates the quality of the synthesized core-shell NPs. More TEM micrographs of the core-shell NPs are provided in the Supplementary Material. The size-uniformity of the core-shell NPs is a result of the narrow particle size of the Ag NPs. Hydrodynamic sizes of the core and the core-shell NPs are compared in Figure 5b. Table 2 presents a list of the size and other properties of the Ag core and $Ag@SiO_2$ core-shell NPs.

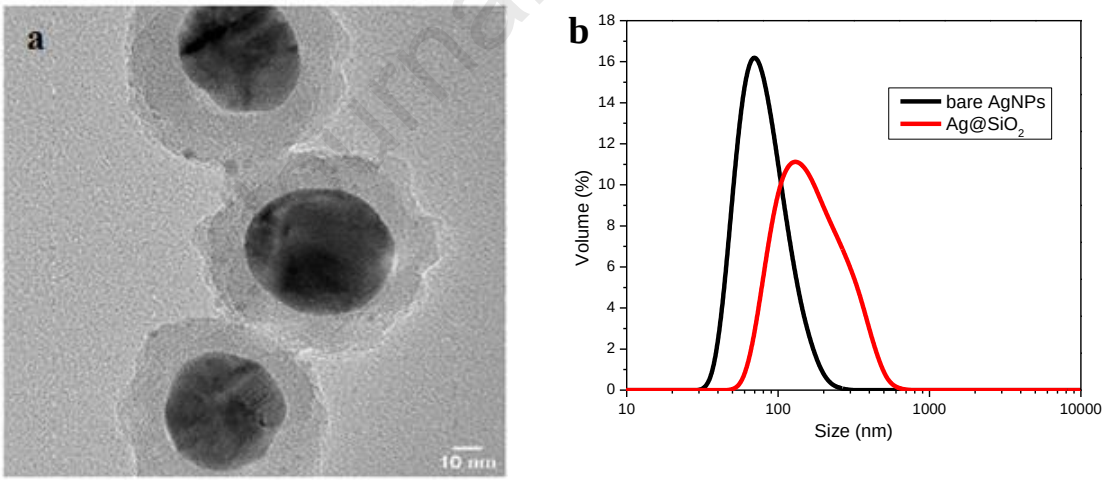

Figure 5: a) TEM images of core-shell $Ag@SiO_2$NPs; and b) particle size distribution of AgNPs and $Ag@SiO_2$NPs by DLS

Table 2: Physical properties of synthesized AgNPs and $Ag@SiO_2$NPs.

NPs	UV-Vis		DLS		SEM, ImageJ size (nm)	Zeta potential in ethanol (mV)*
	SPR peak (nm)	FWHM (nm)	Size (nm)	PDI		
Bare Ag	436	97	68	0.153	54	+13
$Ag@SiO_2$	446	130	122	0.141	81	-25

* 9 months after synthesis

Figure 6 shows 8-10 nm particles of SiO_2 that are chained around some $Ag@SiO_2$ NPs. By the completion of the condensation process, these SiO_2 cores become aggregated and then condense to make the surface of the NPs even smoother. Here we expect that, by extending the reaction time (> 18 h), these small particles of SiO_2 will dissolve and precipitate on the surface of the $Ag@SiO_2$ NPs to make the NPs more round through a mechanism known as Ostwald's ripening.

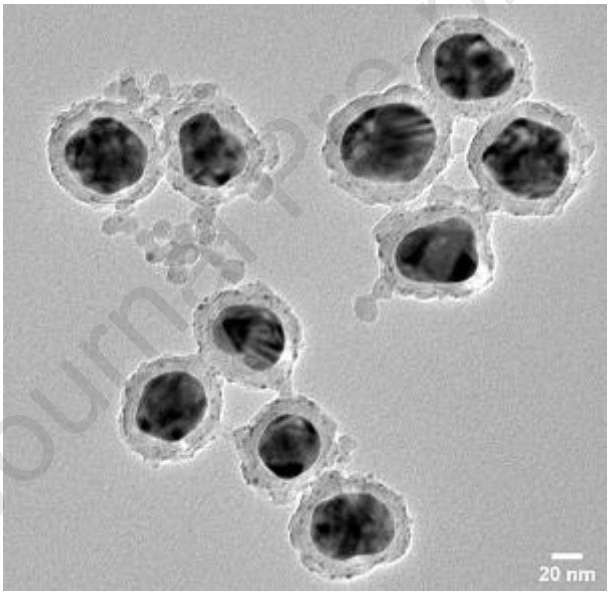

Figure 6: TEM images of $Ag@SiO_2$ NPs showing small SiO_2 NPs.

In order to evaluate the elemental composition of the $Ag@SiO_2$ NPs, EDS analysis was performed at three points, as depicted in Figure 7. The results confirmed the presence of the SiO_2 shell on the surface of the AgNPs. Zeta potential confirmed this too. Resulted from surface variation of the NPs, the zeta potential provides some information about the suspension-stability of the NPs and the states of the surface charges [51]. According to Table 2, the zeta potential in ethanol was measured at +13 mV and -25 mV for the Ag and $Ag@SiO_2$ NPs, respectively. This large negative value for the Ag NPs coated with SiO_2 indicated the success of the coating providing a great repulsive force between the particles, which enhanced the stability of the NPs and prevented their agglomeration.

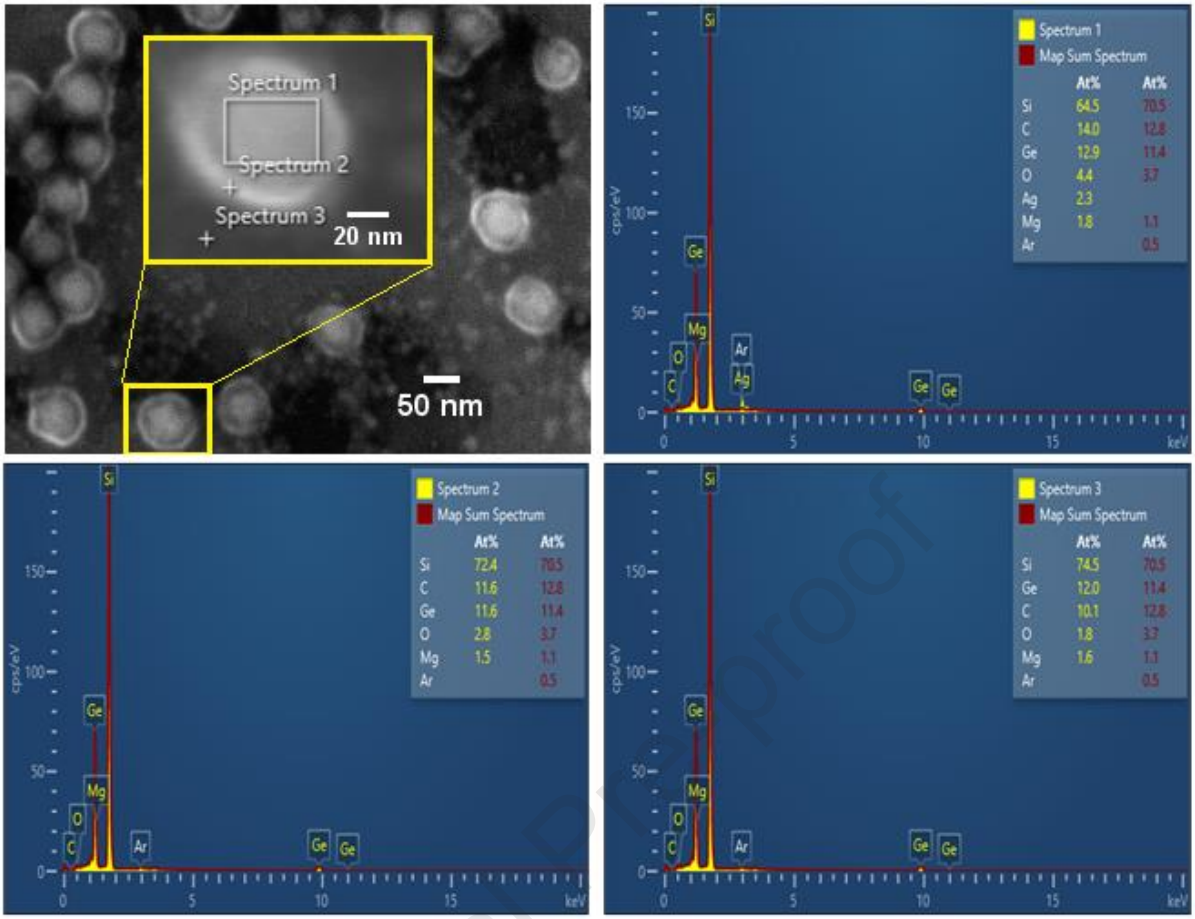

Figure 7: SEM micrograph and EDS analysis in three point of Ag@SiO_2 NPs.

Figure 8 shows the optical absorption peaks of the Ag and Ag@SiO_2 NPs. A clear red-shift in the position of the SPR absorption peak is seen from 432 to 446 nm, which agrees well with the earlier reports [52-58].

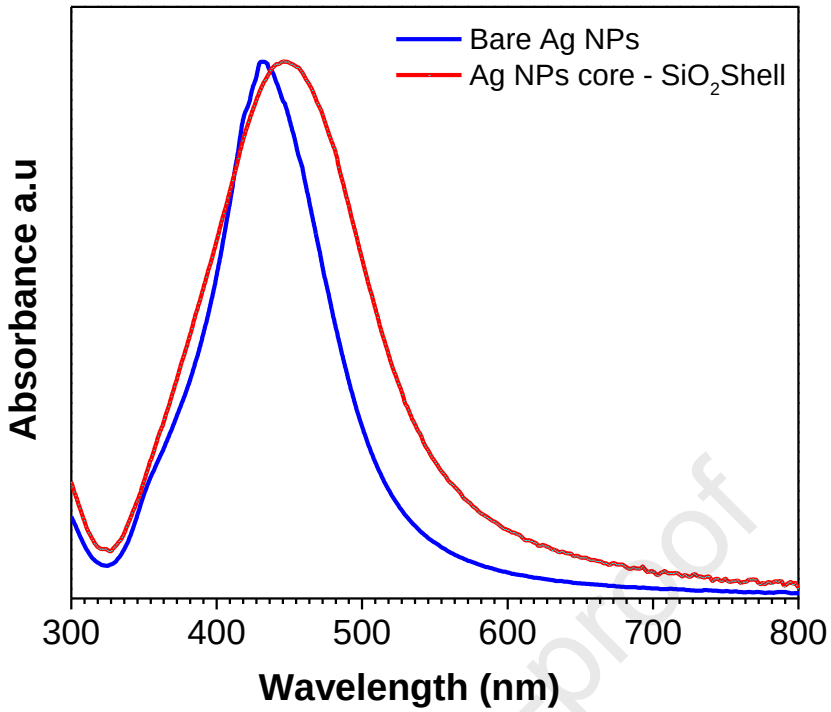

Figure 8: UV-Vis spectra of Ag core and core-shell Ag@SiO_2 NPs.

In core-shell NPs, the metal core plasmon peak wavelength can be expressed as follows [59, 60]:

$$\lambda = \lambda_p \left(\varepsilon^{\infty} + 2n_m^2 + \frac{2g(n_s^2 - n_m^2)}{3} \right)^{\frac{1}{2}} \qquad (11)$$

where n_m is the refractive index of the host medium, n_s is the refractive index of the shell, ε^{∞} is the high-frequency optical dielectric constant of the metallic core, g is the volumetric fraction of the shell layer, λ is the estimated position of the plasmon peak for the metallic core, and λ_p is wavelength of the plasmon peak for the bulk metal, which the latter parameter being dependent on the effective mass and density of the free electrons of the metallic core.

Equation (11) suggests that dependence of the plasmon resonance on the refractive index of the material around the surface of the metallic particle and the thickness of the dielectric shell encompassing the particle. The LSPR wavelength increases with the refractive index of the medium hosting the NPs. This increase can be attributed to the improved shielding effect of the electric field with increasing the refractive index, which is known to add to the coulombic force between the electron clouds and the positively charged ions and the resultant decrease in the excitation energy of the electrons on the surface of the NPs [34]. This red-shift increases until the oscillator-induced electric field is fully encompassed within the silica shell [61]. As observed in Figure 8, the FWHM changed from 97 nm for the bare Ag NPs to 130 nm for the core-shell Ag@SiO_2 NPs. This slight change highlights the uniform thickness of the SiO_2 shell [62] and absence of multi-core core-shell complexes.

Altering the optical properties of the Ag NPs, the SiO_2 coating modifies the characteristics of the interface between the Ag NPs and the surrounding medium, easing the adjustment of the plasmonic wavelength and the electric field intensity [18, 63]. Figure 9 shows the variations of the effective dielectric constant of a layer of polymer with a refractive index of 1.5 containing core-shell $Ag@SiO_2$ NPs at different volumetric fraction at wavelength of 400 nm, as derived from the Clausius - Mossotti equation. As is evident from Figure 9, the $Ag@SiO_2$ NPs with the synthesized particle sizes could generate epsilon negative species in the visible range (red curves). In addition, further simulations can be done to determine the number and thickness of polymer layers for obtaining particular optical properties and manipulating the light. Therefore, the proposed core-shell NPs, composed of 54nm Ag NPs coated with 10nm SiO_2 shell, is a promising candidate for metamaterial and metasurface applications.

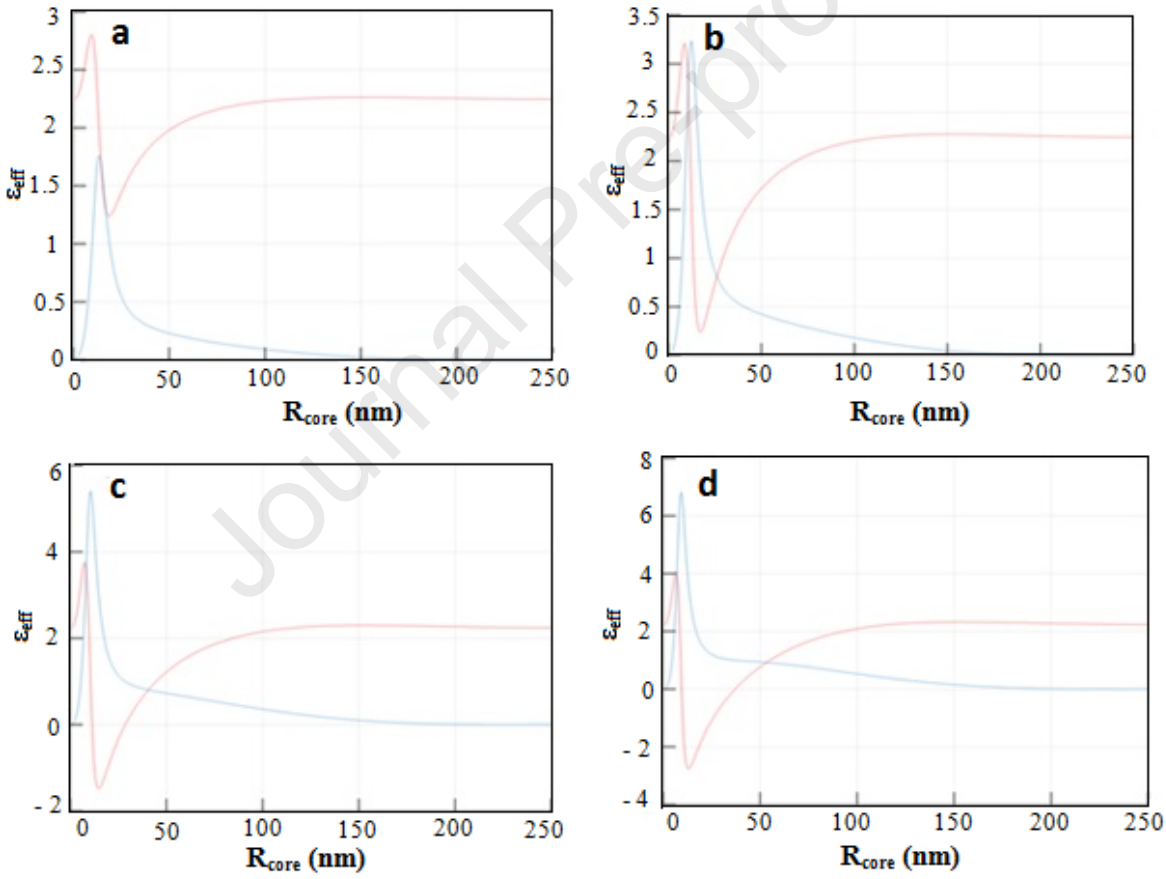

Figure 9: Effective dielectric constant changes in a layer of a polymer with refractive index of 1.5 containing $Ag@SiO_2$ NPs with 10 nm shell thickness and different core size at wavelengths of 400nm with filling fraction of; a) 0.05, b) 0.1, c) 0.2, and d) 0.3.

Conclusions

Various surface effects on the optical behavior of the Ag NPs synthesized through MW-assisted polyol method were investigated. Firstly, the effect of surface area was studied by UV-Vis spectroscopy for the Ag NPs with average particle size of 30, 54, and 61 nm. The results indicated a red-shift in the absorption wavelength with increasing size of Ag NPs. Knowing that smaller particles tend to support limited-amplitude plasmonic oscillations and an increase in the size of the Ag NPs induces a larger electric field in the vicinity of the NPs, the 54nm Ag NPs were selected for further investigating the surface effects. As a controlled dielectric medium, a coating of silica was formed around the Ag NPs. The process design was performed by the Clausius - Mossotti equation, and the results indicated the appropriateness of a SiO_2 shell with a thickness of 10 nm for establishing ENM in a polymer layer. The shell was grown by the Stöber process. TEM analysis confirmed the formation of a uniform shell around the Ag NPs, with the red-shift of the absorption peak after the shell formation and the results of EDS analysis further confirming the formation of SiO_2 shell. The large negative zeta potential for the $Ag@SiO_2$ NPs showed good stability of the core-shell NPs compared to the bare Ag NPs. The $Ag@SiO_2$ NPs can be used in polymer layers for developing metasurfaces for many plasmonic applications.

Declarations of interest: none

References

[1] O.A. Yeshchenko, et al., Size-dependent surface-plasmon-enhanced photoluminescence from silver nanoparticles embedded in silica, Phys Rev B. 79 (2009) 235438; doi: 10.1103/PhysRevB.79.235438

[2] K. N′Konou, et al., Impact of $Ag@SiO_2$ core-shell nanoparticles on the photoelectric current of plasmonic inverted organic solar cells, Synthetic Met. 239 (2018) 22-28; https://doi.org/10.1016/j.synthmet.2018.03.003

[3] J. Lee, et al., Size-dependent plasmonic effects of M and $M@SiO_2$ (M = Au or Ag) deposited on TiO_2 in photocatalytic oxidation reactions, Appl Catal B-Environ. 214 (2017) 15-22; http://dx.doi.org/10.1016/j.apcatb.2017.05.025

[4] D. Ganeshan, et al., Plasmonic effects of silver nanoparticles embedded in the counter electrode on enhanced performance of dye-sensitized solar cells, Langmuir 34 (2018) 5367-5373; https://doi.org/10.1021/acs.langmuir.7b03086

[5] T. Lünskens, et al., Plasmons in supported size-selected silver nanoclusters, Phys Chem Chem Phys. 17 (2015) 17541; doi: 10.1039/c5cp01582k

[6] A. Monti, et al., Optical invisibility through metasurfaces made of plasmonic nanoparticles, J Appl Phys 117 (2015) 123103; doi: 10.1063/1.4916257

[7] N.M. Bahadur, et al., Fast and facile synthesis of silica coated silver nanoparticles by microwave irradiation, J Colloid Inter Sci. 355 (2011) 312-320; doi: 10.1016/j.jcis.2010.12.016

[8] Z. Lalegani, et al., Modeling, design, and synthesis of gram-scale monodispersed silver nanoparticles using microwave-assisted polyol process for metamaterial applications, Opt Mater. 108 (2020) 110381; doi: https://doi.org/10.1016/j.optmat.2020.110381

[9] S. Raj, P. Rai, Y. Yu, Pulse electrophoresis deposition of Ag@SiO_2 core-shell nanoparticles on FTO substrate, Mater Lett. 117 (2014) 116-119; http://dx.doi.org/10.1016/j.matlet.2013.11.123

[10] K. Aslan, et al., Fluorescent core-shell Ag@SiO_2 nanocomposites for metal-enhanced fluorescence and single nanoparticles sensing platforms, J Am Chem Soc. 129 (2007) 1524-1525; doi: 10.1021/ja0680820

[11] T. Jin, et al., Ag@SiO_2 nanoparticles performing as a nanoprobe for selective analysis of 2-aminoanthracene in wastewater samples via metal-enhanced fluorescence, Talanta 200 (2019) 242-248; https://doi.org/10.1016/j.talanta.2019.03.054

[12] Q. Wu, et al., Preparation of Ag@SiO_2@NH_2 core-shell nanocomposites for the fluorescence enhancement of carbon quantum dots, J Nanopart Res 21 (2019) 259; https://doi.org/10.1007/s11051-019-4676-1

[13] Y. Chang, Y. Lu, K. Chou, Enhancement of photoluminescence of different quantum dots by Ag@SiO_2 core-shell nanoparticles, Mater Res Bull. 48 (2013) 2076-2078; http://dx.doi.org/10.1016/j.materresbull.2013.02.032

[14] L. Kong, et al., Fluorescence enhancement of europium nitrobenzoates by Ag@SiO_2 nanoparticles in solution, J Lumin. 186 (2017) 255-261; http://dx.doi.org/10.1016/j.jlumin.2017.02.044

[15] B. Yun, et al., Highly sensitive metal-enhanced fluorescence biosensor prepared on electrospun fibers decorated with silica-coated silver nanoparticles, Sensor Actuat B-Chem. 284 (2019) 140-147; https://doi.org/10.1016/j.snb.2018.12.096

[16] S. Krishnan, et al., Dual labeled Ag@SiO_2 core-shell nanoparticles based optical immunosensor for sensitive detection of *E. coli*, Mat Sci Eng C-Mater. 45 (2014) 337-342; http://dx.doi.org/10.1016/j.msec.2014.09.028

[17] V. Amendola, Surface Plasmon resonance of silver and gold nanoparticles in the proximity of graphene studied using the discrete dipole approximation method, Phys Chem Chem Phys. 18 (2016) 2230-2241; doi: 10.1039/c5cp06121k

[18] A. Nagarajan, et al., Optimization of electric field enhancement of Ag@SiO_2 trimer nanospheres by finite difference time domain method, Appl Surf Sci. 495 (2019) 143547; https://doi.org/10.1016/j.apsusc.2019.143547

[19] K. Niciński, et al., Detection of circulating tumor cells in blood by shell-isolated nanoparticles-enhanced Raman spectroscopy (SHINERS) in microfluidic device, Sci Rep-UK 9 (2019) 9267; https://doi.org/10.1038/s41598-019-45629-7

[20] R. Paniagua-Domínguez, et al., Metallo-dielectric core-shell nanospheres as building blocks for optical three-dimensional isotropic negative-index metamaterials, New J Phys 13 (2011) 123017; http://iopscience.iop.org/1367-2630/13/12/123017

[21] E. Donnelly, L. La Spada, Electromagnetic and thermal nanostructures: from waves to circuits, Engineering Research Express 2 (2020) 015045; https://doi.org/10.1088/2631-8695/ab7a78

[22] L. La Spada, L. Vegni, Electromagnetic nanoparticles for sensing and medical diagnostic applications, Materials 11 (2018) 603; doi: 10.3390/ma11040603

[23] A. Sihvola, Electromagnetic Mixing Formulas and Applications. London: The Institution of Engineering and Technology (2008).

[24] H. He, et al., Controllably prepared molecularly imprinted core-shell plasmonic nanostructure for plasmon-enhanced fluorescence assay, Biosens Bioelectron. 146 (2019) 111733; https://doi.org/10.1016/j.bios.2019.111733

[25] W. Stöber, A. Fink, E. Bohn, Controlled growth of monodisperse silica spheres in the micron size range, J Colloid Interface Sci 26 (1968) 62-69; doi: https://doi.org/10.1016/0021-9797(68)90272-5

[26] V. Amendola, O.M. Bakr, F. Stellacci, A study of the surface Plasmon resonance of silver nanoparticles by the discrete dipole approximation method: effect of shape, size, structure, and assembly, Plasmonics 5 (2010) 85-97; doi: 10.1007/s11468-009-9120-4

[27] W. Hergert, T. Wriedt (eds.), The Mie Theory, Springer Series in Optical Sciences 169 P:53-71; doi: 10.1007/978-3-642-28738-1_2

[28] D. Acharya, B. Mohanta, Optical properties of synthesized Ag and Ag@SiO_2 core-shell nanoparticles, AIP Conference Proceedings 1832 (2017) 050155; doi: 10.1063/1.4980388

[29] J. Montaño-Priede, O. Rodríguez, U. Pal, Near-electric field tuned plasmonic Au@SiO_2 and Ag@SiO_2 nanoparticles for efficient utilization in luminescence enhancement and surface enhanced spectroscopy, J Phys Chem C. 41 (2017) 23062-23071; https://doi.org/10.1021/acs.jpcc.7b07395

[30] K. Lee, et al., Size effect of Ag nanoparticles on surface Plasmon resonance, Surf Coat Tech. 202 (2008) 5339-5342; doi:10.1016/j.surfcoat.2008.06.080

[31] W. Ho, S. Fen, J. Liu, Plasmonic effects of silver nanoparticles with various dimensions embedded and non-embedded in silicon dioxide antireflective coating on silicon solar cells, Appl Phys A. 124 (2018) 29; https://doi.org/10.1007/s00339-017-1451-y

[32] L. Genzel, T.P. Martin, U. Kreibig, Dielectric function and plasma resonances of small metal particles, Z Physik B 21 (1975) 339-346; https://doi.org/10.1007/BF01325393

[33] S.L. Smitha, et al., Studies on surface Plasmon resonance and photoluminescence of silver nanoparticles, Spectrochim Acta A. 71 (2008) 186-190; doi: 10.1016/j.saa.2007.12.002

[34] M. Shabaninezhad, G. Ramakrishna, Theoretical investigation of plasmonic properties of quantum-sized silver nanoparticles, Plasmonics 15 (2020) 783-792; https://doi.org/10.1007/s11468-019-01102-9

[35] J. Tiggesbäumker, et al., Blue shift of the Mie plasma frequency in Ag clusters and particles, Phys Rev A 48 (1993) R1749; https://doi.org/10.1103/PhysRevA.48.R1749

[36] A. Hilger, et al., Surface and interface effects in the optical properties of silver nanoparticles, Eur Phys J D 10 (2000) 115-118; https://doi.org/10.1007/s100530050531

[37] Y. Wei, et al., The effect of silica shell on the surface enhanced Raman scattering and fluorescence with Ag nanoparticles: a three-dimensional finite element method investigation, Opt Commun. 427 (2018) 426-432; https://doi.org/10.1016/j.optcom.2018.06.086

[38] F. Mafune´, et al., Structure and stability of silver nanoparticles in aqueous solution produced by laser ablation, J Phys Chem B 104 (2000) 8333-8337; doi: 10.1021/jp001803b

[39] J. Alimunnisa, K. Ravichandran, K.S. Meena, Synthesis and characterization of Ag@SiO_2 core-shell nanoparticles for antibacterial and environmental applications, J Mol Liq. 231 (2017) 281-287; http://dx.doi.org/10.1016/j.molliq.2017.01.103

[40] A. Yuksel, et al., Near-field plasmonic of gold nanoparticles in dielectric media, J Quant Spectrosc Ra 254 (2020) 107207; doi: https://doi.org/10.1016/j.jqsrt.2020.107207

[41] refractiveindex.info

[42] I. H. Malitson, Interspecimen comparison of the refractive index of fused silica, Josa, 55:10 (1965) 1205-1209; https://doi.org/10.1364/JOSA.55.001205

[43] K. M. McPeak, S. V. Jayanti, S. J. Kress, S. Meyer, S. Iotti, A. Rossinelli, & D. J. Norris, Plasmonic films can easily be better: rules and recipes, ACS photonics, 2:3 (2015) 326-333; https://doi.org/10.1021/ph5004237

[44] O. Niitsoo, A. Couzis, Facile synthesis of silver core – silica shell composite nanoparticles, J Colloid Inter Sci. 354 (2011) 887-890; doi:10.1016/j.jcis.2010.11.013

[45] M. Lismont, C. A.Páez, L. Dreesen, A one-step short-time synthesis of $Ag@SiO_2$ core-shell nanoparticles, J Colloid Inter Sci. 447 (2015) 40-49; http://dx.doi.org/10.1016/j.jcis.2015.01.065

[46] D. Donatti, D. Vollet, Effects of the water quantity on the solventless TEOS hydrolysis under ultrasound stimulation, J Sol-gel Sci Techn. 17 (2000) 19-24; https://doi.org/10.1023/A:1008748702656

[47] S. Raj, et al., Morphology controlled $Ag@SiO_2$ core-shell nanoparticles by ascorbic acid reduction, J Mater Sci: Mater Electron 25 (2014) 1156-1161; doi:10.1007/s10854-013-1702-4

[48] L. Rainville, M. Dorais, D. Boudreau, Controlled synthesis of low polydispersity $Ag@SiO_2$ core-shell nanoparticles for use in plasmonic applications, RSC Adv. 3 (2013) 13953; doi: 10.1039/c3ra41677a

[49] S. Liu, M. Han, Silica-coated metal nanoparticles, Chem. Asian J. 5 (2010) 36-45; DOI: 10.1002/asia.200900228

[50] Y. Wang, et al., Enhanced efficiency of perovskite solar cells by using core-ultrathin shell structure $Ag@SiO_2$ nanowires as plasmonic antennas, Adv. Electron. Mater. 3 (2017) 1700169; doi: 10.1002/aelm.201700169

[51] M. Rodrigues, et al., Biogenic synthesis and antimicrobial activity of silica-coated silver nanoparticles for esthetic dental applications, J Dent. 96 (2020) 103327; https://doi.org/10.1016/j.jdent.2020.103327

[52] S.V. Otari, et al., Facile one pot synthesis of core shell $Ag@SiO_2$ nanoparticles for catalytic and antimicrobial activity, Mater Lett. 167 (2016) 179-182; https://doi.org/10.1016/j.matlet.2015.12.134

[53] K.I. Dhanalekshmi, et al., Preparation and characterization of core-shell type $Ag@SiO_2$ nanoparticles for photodynamic cancer therapy, Photodiagn Photodyn. 28 (2019) 324-329; https://doi.org/10.1016/j.pdpdt.2019.10.006

[54] P. Massé, et al., Synthesis of size-monodisperse spherical $Ag@SiO_2$ nanoparticles and 3-D assembly assisted by microfluidics, Langmuir 29 (2013) 1790-1795; dx.doi.org/10.1021/la3039335

[55] A. Campos, et al., Plasmonic quantum size effects in silver nanoparticles are dominated by interfaces and local environments, Nat Phys. 15 (2019) 275-280; https://doi.org/10.1038/s41567-018-0345-z

[56] J. Kang, et al., Core-shell $Ag@SiO_2$ nanoparticles of different silica shell thicknesses: preparation and their effects on photoluminescence of lanthanide complexes, Mater Res Bull. 71 (2015) 116-121; http://dx.doi.org/10.1016/j.materresbull.2015.07.017

[57] W. Wang, et al., $Ag@SiO_2$ core-shell nanoparticles for probing spatial distribution of electromagnetic field enhancement *via* surface-enhanced Raman scattering, ACS Nano 3 (2009) 3493-3496; doi: 10.1021/nn9009533

[58] K.I. Dhanalekshmi, K.S. Meena, Comparison of antibacterial activities of $Ag@TiO_2$ and $Ag@SiO_2$ core-shell nanoparticles, Spectrochim Acta A 128 (2014) 887-890; http://dx.doi.org/10.1016/j.saa.2014.02.063

[59] T. Hirakawa, P. Kamat, Charge separation and catalytic activity of $Ag@TiO_2$ core-shell composite clusters under UV-irradiation, J Am Chem Soc. 127 (2005) 3928-3934; doi: 10.1021/ja042925a

[60] A. Templeton, et al., Solvent refractive index and core charge influences on the surface plasmon absorbance of alkanethiolate monolayer-protected gold clusters, J Phys Chem B 104 (2000) 564-570; 10.1021/jp991889c

[61] J. Asselin, et al., Correlating metal-enhanced fluorescence and structural properties in $Ag@SiO_2$ core-shell nanoparticles, Plasmonics 11 (2016) 1369-1376; doi: 10.1007/s11468-016-0186-5

[62] J. Kang, et al., Tuning the luminescence properties of samarium and dysprosium complexes by $Ag@SiO_2$ nanoparticles, J Photoch Photobio A 365 (2018) 119-124; https://doi.org/10.1016/j.jphotochem.2018.07.030

[63] Y. Hu, et al., Scalable preparation of ultrathin silica-coated Ag nanoparticles for SERS application, ACS Appl Mater Inter. 5 (2013) 10643-10649; dx.doi.org/10.1021/am402604h

Highlights

- The effect of various parameters on effective dielectric constant mapped using RSM.
- Controlled and uniform silica spacer formed around AgNPs.
- A polymeric layer with negative epsilon designed using synthesized Ag@SiO_2 NPs.

Z. Lalegani : Investigation, Methodology, Validation, Writing - Original Draft, Visualization.

S.A. Seyyed Ebrahimi : Supervision, Conceptualization, Project administration, Resources, Writing - Review & Editing.

B. Hamawandi : Data Curation, Formal analysis.

L. La Spada : Software.

H. Batili : Data Curation.

M. S. Toprak : Conceptualization, Resources, Writing - Review & Editing.

Declaration of interests

☑The authors declare that they have no known competing financial interests or personal relationships that could have appeared to influence the work reported in this paper.

☐The authors declare the following financial interests/personal relationships which may be considered as potential competing interests: